



# The geochemistry and sequestration of H<sub>2</sub>S into the geothermal system at Hellisheidi, Iceland

Andri Stefánsson<sup>a,\*</sup>, Stefán Arnórsson<sup>a</sup>, Ingvi Gunnarsson<sup>b</sup>, Hanna Kaasalainen<sup>a</sup>, Einar Gunnlaugsson<sup>b</sup>

<sup>a</sup> Institute of Earth Sciences, University of Iceland, Sturlugata 7, 101 Reykjavík, Iceland

<sup>b</sup> Reykjavik Energy, Baejarhals 1, 110 Reykjavík, Iceland

## ARTICLE INFO

### Article history:

Received 5 May 2010

Accepted 23 December 2010

Available online 3 January 2011

### Keywords:

geothermal  
hydrogen sulphide  
geochemical modelling  
sequestration

## ABSTRACT

The geochemistry and mineralization of H<sub>2</sub>S in the geothermal system hosted by basaltic rock formation at Hellisheidi, SW Iceland, was studied. Injection of mixtures of H<sub>2</sub>S with geothermal waste water and condensed steam into the >230 °C geothermal aquifer is planned, where H<sub>2</sub>S will hopefully be removed in the form of sulphides. The natural H<sub>2</sub>S concentrations in the aquifer average 130 ppm. They are considered to be controlled by close approach to equilibrium with pyrite, pyrrhotite, prehnite and epidote. Injection of H<sub>2</sub>S will increase significantly the reservoir H<sub>2</sub>S equilibrium concentrations, resulting in mineralization of pyrite and possibly other sulphides as well as affecting the formation of prehnite and epidote. Based on reaction path modelling, the main factors affecting the H<sub>2</sub>S mineralization capacity are related to the mobility and oxidation state of iron. At temperatures above 250 °C the pyrite mineralization is greatly reduced upon epidote formation leading to the much greater basalt dissolution needed to sequester the H<sub>2</sub>S. Based on these findings, the optimum conditions for H<sub>2</sub>S injection are aquifers with temperatures below ~250 °C where epidote formation is insignificant. Moreover, the results suggest that sequestration of H<sub>2</sub>S into the geothermal system is feasible. The total flux of H<sub>2</sub>S from the Hellisheidi power plant is 12,950 tonnes yr<sup>-1</sup>. Injection into 250 °C aquifers would result in dissolution of ~1000 tonnes yr<sup>-1</sup> of basalt for mineralization of H<sub>2</sub>S as pyrite, corresponding to ~320 m<sup>3</sup> yr<sup>-1</sup>.

© 2011 Elsevier B.V. All rights reserved.

## 1. Introduction

Hydrogen sulphide (H<sub>2</sub>S) is among the major components in geothermal fluids, with concentrations ranging from a few ppb to levels of hundreds of ppm (Arnórsson 1995a, 1995b). Hydrogen sulphide is volatile and is commonly emitted into the atmosphere from geothermal power plants, causing potential environmental problems.

Several methods are employed in cleaning H<sub>2</sub>S emissions including oxidation to form elemental sulphur or sulphuric acid (Sanopoulos and Karabelas, 1997). One method includes injection of H<sub>2</sub>S into geothermal systems where it may be mineralized into sulphides including pyrite. Reykjavik Energy, Iceland, is currently planning such an injection into the Hellisheidi geothermal system, where geothermal gas (CO<sub>2</sub>, H<sub>2</sub>S, N<sub>2</sub> and H<sub>2</sub>) will be separated in a gas abatement station and the H<sub>2</sub>S stream mixed at the surface with current injection fluids consisting of geothermal waste water (92%) and condensed steam (8%) and subsequently injected into the >230 °C geothermal aquifer. The stream of CO<sub>2</sub> will, on the other hand, be mixed with non-thermal ground waters and injected into >50 °C aquifers (Matter et al., 2009; Gíslason et al., 2010).

It is generally accepted that the major elemental composition including H<sub>2</sub>S concentration of geothermal fluids is controlled by local equilibrium with common secondary minerals (e.g. Giggenbach, 1980, 1981; Arnórsson et al., 1983; Stefánsson and Arnórsson, 2000; Gudmundsson and Arnórsson, 2005). For H<sub>2</sub>S the secondary minerals considered to be involved at low salinity (<1000 ppm Cl) and temperatures above ~230 °C are pyrite, pyrrhotite, prehnite and epidote as well as possibly magnetite (Stefánsson and Arnórsson, 2002). Therefore, elevated H<sub>2</sub>S concentrations may lead to sulphide mineralization as well as some iron oxide and aluminium silicate formation. However, the exact response of the system, including the rate and quantity of H<sub>2</sub>S mineralization, redox reactions and the associated fluid chemistry, is somewhat unclear.

Previous work on volatile gas disposal has mainly focused on reaction modelling and experiments regarding CO<sub>2</sub> and SO<sub>2</sub> or H<sub>2</sub>S in addition to CO<sub>2</sub> (e.g. Gunter et al., 2000; Johnson et al., 2001; McPherson and Lichtner, 2001; Xu et al., 2004; Knauss et al., 2005; White et al., 2005; Xu et al., 2005; Zerai et al., 2006; Xu et al., 2007; Jacquemet et al., 2008; Palandri and Kharaka, 2008; Crandell et al., 2010) and fluid–rock interaction in geothermal systems under natural conditions, both in a static way (e.g. Giggenbach, 1981; Arnórsson et al., 1983; Gudmundsson and Arnórsson, 2005) and applying reactive transport modelling (e.g. Xu et al., 2006; Gessner et al., 2009). However, less is known about H<sub>2</sub>S disposal under geothermal

\* Corresponding author.

E-mail address: [as@hi.is](mailto:as@hi.is) (A. Stefánsson).

conditions. There are considerable geochemical uncertainties related to injection and sequestration of H<sub>2</sub>S, including the effects of H<sub>2</sub>S supply on the fluid–rock interaction, rate and mechanism of H<sub>2</sub>S mineralization, and oxidation kinetics of H<sub>2</sub>S under geothermal conditions.

In order to evaluate the geochemical effects of the injection of H<sub>2</sub>S charged injection waters into geothermal systems, sets of geochemical modelling calculations were carried out. These involved two steps, firstly evaluating the geochemistry of H<sub>2</sub>S in the Hellisheidi geothermal system and secondly, carrying out calculations of H<sub>2</sub>S–water–rock interaction under geothermal conditions.

## 2. The Hellisheidi geothermal system

The Hengill geothermal area is situated at the junction of the North American plate, Eurasian plate and the Hreppar microplate (Foulger, 1988; Sigmundsson et al., 1997) in SW Iceland. At present, two geothermal power plants are being operated in the area, the Nesjavellir and Hellisheidi geothermal power plants. At Nesjavellir 25 wells have been drilled and the installed power capacity is 120 MW electric and 300 MW thermal. At Hellisheidi, about 50 wells have been drilled and the power production is 180 MW electric by high pressure turbines and 33 MW electric by a low pressure turbine. The currently planned H<sub>2</sub>S injection is into the Hellisheidi geothermal system.

The rock types associated with the geothermal system of the Hengill area are composed of layers of basaltic hyaloclastites, lava flows and intrusions, mostly of tholeiite and olivine tholeiite composition with minor intermediate rocks and rhyolites. The primary mineralogy consists of olivine and plagioclase phenocrysts with plagioclase, augite, olivine, Ti–Fe oxides and glass in the groundmass (Sæmundsson, 1967, 1992).

The alteration mineralogy of some of the wells drilled into the systems has been extensively studied (e.g. Schiffman and Fridleifsson, 1991; Larsson et al., 2002). Four zones have been characterized with smectites and zeolites at <200 °C, a zone of mixed layer clays at 200–250 °C, a chlorite–epidote zone at 250–300 °C and an epidote–actinolite zone at >300 °C (Fridleifsson, 1991). The main zeolite observed at >120 °C is analcime with wairakite appearing at >180 °C. Calcite and pyrite are stable at all temperatures except at the deepest levels at Nesjavellir (>300 °C). Chalcedony forms up to temperatures of about 200 °C where it is replaced by quartz (Kristmannsdóttir, 1979). Albite is commonly identified and becomes abundant at temperatures exceeding 150 °C. K-feldspar, on the other hand, is not common, probably resulting from the low potassium content of the basalts (Larsson et al., 2002). Prehnite becomes stable above 200 °C and epidote at slightly higher temperatures (Kristmannsdóttir, 1979). Actinolite becomes the predominant secondary mineral above 280 °C (Hreggvidsdóttir, 1987). In addition, hornblende and garnet have been identified at the highest temperatures (Hreggvidsdóttir, 1987). The clays predominating at low temperatures are smectites rich in Fe and Mg. At about 200 °C they are replaced by a regularly or randomly interstratified smectite–chlorite (Schiffman and Fridleifsson, 1991) whereas discrete chlorite forms at temperatures of 230–240 °C (Kristmannsdóttir, 1979). Sometimes the geothermal mineralogy does not match with the present temperature conditions. This is considered to result from temperature changes in the geothermal systems with the secondary mineralogy, at least partly, representing past temperature conditions.

The gas concentration in the steam from the Hellisheidi power plant is on average 0.506 wt.%. Of this 73.2% is CO<sub>2</sub>, 23.5% H<sub>2</sub>S, 2.0% N<sub>2</sub>, 0.79% H<sub>2</sub>, 0.46% Ar and 0.06% CH<sub>4</sub> on a molal scale. The steam flow at the power plant is 345 kg s<sup>-1</sup>, which is consistent with 1.9 kg s<sup>-1</sup> steam needed to produce 1 MW electric. Based on these figures, the total flux of H<sub>2</sub>S from the Hellisheidi power plant is ~12,950 tonnes yr<sup>-1</sup> for 180 MW electric produced by the high pressure turbines (Table 1).

**Table 1**

Gas composition and fluxes from Hellisheidi power plant, SW Iceland.

Gas	wt.% gas	tonnes yr <sup>-1</sup>	
		180 MWe	270 MWe
CO <sub>2</sub>	0.37 ± 0.07	42,000	60,300
H <sub>2</sub> S	0.12 ± 0.01	12,950	18,900
Ar	0 ± 0	250	380
N <sub>2</sub>	0.01 ± 0.01	1100	1650
CH <sub>4</sub>	0 ± 1.00E–04	30	45
H <sub>2</sub>	0 ± 7.00E–04	125	640
wt.% total gas	0.51 ± 0.07		

## 3. Database and data handling

### 3.1. Sampling and analysis

A total of 11 samples were collected of geothermal fluids, steam and water at the Hellisheidi geothermal system in 2008. The sampling and analytical procedures are described in detail by Arnórsson et al. (2006).

The steam and water phases were separated using a Webre separator. Steam samples were collected into 200 ml pre-evacuated gas bulbs containing 5–10 ml 50% KOH solution. The concentrations of CO<sub>2</sub> and H<sub>2</sub>S in the steam condensate were analysed by several methods. CO<sub>2</sub> was analysed using modified alkalinity titration and using ion chromatography (IC) after dilution (Stefánsson et al., 2007). H<sub>2</sub>S was analysed using Hg precipitation titration (Arnórsson et al., 2006) and as SO<sub>4</sub> using IC after oxidation with H<sub>2</sub>O<sub>2</sub> and UV digestion. All the methods compared within uncertainties. The analytical precision at the 95% confidence level based on duplicate analysis was <3%.

The water samples for major elemental analysis were filtered on site through 0.2 µm filters (cellulose acetate) into polypropylene bottles. Samples for major cation analysis were acidified with concentrated HNO<sub>3</sub> (Suprapure, Merck), 0.5 ml acid to 100 ml sample, and analysed using ICP-OES.

Several methods were applied for analysis of pH, H<sub>2</sub>S and SO<sub>4</sub> in the water phase. The pH was analysed on site at ~20 °C. The water flow from the Webre separator was cooled down in-line using two cooling spirals. A T piece was added to the end of the second cooling spiral where part of the flow went to waste and part to a flow-through electrode cell. In this way the pH could be determined using a well calibrated pH electrode at ~20 °C in a closed system within 1–2 min from discharge. The pH was further analysed in the laboratory within 1–2 days of sampling. The laboratory values showed systematically higher pH values (more alkaline). This is considered to result from silica polymerization upon storage (Gunnarsson and Arnórsson, 2008). It is therefore important to measure pH on site for samples with elevated SiO<sub>2</sub> concentrations. The analysis of H<sub>2</sub>S in the water phase was carried out using two methods; firstly, using on site titration with mercury acetate and dithizone as an indicator (Arnórsson et al., 2006) and secondly by using the methylene blue method where the reagents were added to the sample on site followed by analysis in the laboratory. The two methods gave comparable results, within ±5%. The concentration of SO<sub>4</sub> in the water phase was determined by two methods: firstly, on site using IC together with F, Cl and CO<sub>2</sub> (carbonate carbon) and secondly by precipitation of H<sub>2</sub>S on site using a 2% Zn acetate solution (5 ml to 100 ml sample) followed by filtration and analysis of SO<sub>4</sub> by IC in the laboratory. The two methods gave comparable results, within ±3%.

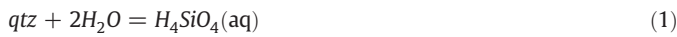
### 3.2. Calculation of aquifer fluid compositions

The calculation of aquifer fluid composition from data on two-phase well discharges (steam and water) collected at the surface

essentially involved two steps, firstly the selection of aquifer reference temperature and secondly the calculation of the aquifer fluid composition and species distribution using an appropriate model.

There are two ways to estimate the temperature beyond the zone of boiling, one to use geothermometers and the other measured downhole temperatures in thermally stabilized well at the depth of permeable horizons. Upon completion of drilling it is common to pump large quantities of cold water into wells. During heating up of the well after completion tests, loss of water shows up as negative temperature peaks, considered to represent permeable horizons. Wells may receive water from more than one aquifer, in which case the discharge is mixed. If the producing aquifers have significantly different temperatures, clearly reconstruction of a single aquifer fluid is not valid. Therefore, it is important to study both the depth level of possible aquifers and their respective temperature measurements as well as geothermometry temperatures that are based on local equilibrium between secondary minerals and the fluids.

In the present work the aquifer temperatures were evaluated and selected based on a combination of measured downhole temperatures and silica and Na/K geothermometer temperatures that are based on local equilibrium between the fluid and quartz (qtz) or low albite (alb) and microcline (mic), respectively, according to the reactions:



For quartz the equilibrium constant was selected from Gunnarsson and Arnórsson (2000) and in the case of alkali-feldspar from Arnórsson and Stefánsson (1999). A summary of the results is given in Table 2.

Aquifers of volcanic geothermal systems penetrated by drill holes may be sub-boiling, i.e. liquid water is only present in the reservoir. In this case, the depth level of first boiling is within the well, at least during the early stages of well discharge when reservoir pressure drawdown is limited, and the system can be approximated as an isolated system. It follows that the aquifer fluid composition may be calculated from:

$$m_i^{d,t} = m_i^{f,t} = m_i^{d,v} x^{d,v} + m_i^{d,l} (1 - x^{d,v}) \quad (3)$$

where  $m_i^{d,t}$  and  $m_i^{f,t}$  represent the concentration of the  $i$ th component in the aquifer fluid and total discharge, respectively,  $m_i^{d,v}$  and  $m_i^{d,l}$  the concentration in the vapour and liquid phases discharged at the surface, and  $x^{d,v}$  is the vapour fraction at surface. However, wells may intersect an aquifer that is two-phase (steam and water), either because this was the natural state of the reservoir or because reservoir drawdown has led to depressurization boiling within an aquifer. Under these conditions the system aquifer wellhead may still act as isolated. It is not common, however, that discharge enthalpy is higher

than that of the aquifer fluid enthalpy beyond the zone of boiling. Depending on the relative permeability effect, depressurization boiling in the aquifer may lead to phase segregation and hence cause increased enthalpy of the discharge well fluids.

Some well discharges at Hellisheidi were observed to have excess enthalpy. The process considered to be responsible for the excess steam fraction at the surface was phase segregation, i.e. a fraction of the liquid water in the aquifer was immobilized by its adhesion to mineral grain surfaces. In this case the concentration of conservative components in the aquifer may be calculated from the expression (Arnórsson et al., 2007),

$$m_r^{f,l} = \frac{m_r^{d,t}}{(1 - x^{f,t})} \left[ V^{f,t} \left( 1 - \frac{1}{1 - x^{e,v}} \right) + \frac{1}{1 - x^{e,v}} \right]^{-1} \quad (4)$$

where  $m_r^{f,l}$  is the concentration of the  $r$ th non-volatile in the aquifer fluid liquid,  $m_r^{d,t}$  the total concentration of the  $r$ th non-volatile component in the well discharge,  $x^{f,t}$  is the aquifer fluid steam fraction, and  $x^{e,v}$  is the mass fraction of steam at  $T^e$ , the selected phase segregation temperature given by

$$x^{e,v} = \frac{h^{f,t} - h^{e,l}}{h^{e,v} - h^{e,l}} \quad (5)$$

where  $h$  stands for enthalpy and the superscripts  $f, t, e, l$  and  $e, v$  for the total fluid and saturated steam and liquid at  $T^e$ .  $V^{f,t}$  is the mass fraction of the initial fluid that has boiled relative to total well discharge given by

$$V^{f,t} = \frac{h^{d,t} - h^{e,l}}{h^{f,t} - h^{e,l}} \quad (6)$$

where  $h$  stands for enthalpy as before and the superscripts  $d, t, e, l$  and  $f, t$  for the total discharge, liquid water at  $T^e$  and total initial aquifer fluid, respectively.

The concentration of volatiles in the aquifer may be calculated from

$$m_s^{f,v} = \frac{m_s^{d,t}}{V^{f,t}} \left[ x^{f,t} \left( 1 - \frac{1}{D_s^f} \right) + \frac{1}{D_s^f} \right]^{-1} \quad (7)$$

where  $m_s^{f,v}$  is the concentration of the  $s$ th volatile in the initial aquifer fluid vapour,  $m_s^{d,t}$  is the total concentration of the  $s$ th volatile in the well discharge,  $x^{f,t}$  is the mass fraction of vapour in the aquifer, and  $D_s^f$  is the distribution coefficient for the  $s$ th volatile between vapour and liquid. In the calculations,  $f v x$  were taken to be zero. In this case  $h^{f,t} = h^{f,l}$  allowing  $V^{f,t}$  to be calculated from Eq. (6) once  $T^f$  and  $T^e$  have been selected. If the

**Table 2**  
Aquifer temperatures in selected wells at Hellisheidi.

Well no	Geothermometers		Well logging (depth/°C)	Dominant aquifers/selected temperatures (°C)
	qtz	Na/K		
HE-07	267	250	920/280, 1265/285	-/280
HE-05	275	260	800/265, 1200/270, 1400/275	1400/275
HE-06	265	245	800/265, 950/270	900/270
HE-11	282	268	950/280	950/280
HE-12	292	267	850/279, 950/280, 1250/295	1250/295
HE-17	288	277	950/275, 1150/290	1150/290
HE-29	303	275	1185/295, 1500/310, 1750/310, 2100/305	1750–2100/300
HE-03	270	266	100/275, 1100/275	1000–1100/275
HE-18	272	253	900/275, 1050/280	900/275
HE-09	297	275	890/270, 1250/305, 1500/320	1250/305

**Table 3**  
Chemical composition for discharge fluids at Hellisheidi, SW Iceland.

Sample no.	08-3001	08-3002	08-3003	08-3004	08-3005	08-3006	08-3007	08-3008	08-3009	08-3010	08-3011 <sup>a</sup>	Low p steam	High p steam
Well no.	HE-07	HE-12	HE-17	HE-11	HE-29	HE-05	HE-06	HE-03	HE-18	HE-09			
Sampling p (bar abs.)	9.5	10.5	11	10.5	9.8	9.8	10.1	10.8	10.4	10.4			
<i>Liquid sample (ppm)</i>													
pH/°C	9.13/17	8.66/19	8.47/17	8.47/17	8.71/21	9.24/20	8.82/21	8.81/19	8.97/19		9.26/20		
H <sub>2</sub> S	76.1	77.4	68.0	55.7	57.5	37.7	56.9	24.3	57.9		34.8		
CO <sub>2</sub>	7.38	10.98	10.55	22.94	11.88	33.12	34.5	4.27	18.85		7.61		
SO <sub>4</sub>	7.54	13.71	5.52	8.57	3.92	19.21	10.35	11.43	8.78		10.81		
Cl	188	182	204	154	101	78	108	366	145		203		
F	1.30	1.36	0.97	1.28	1.97	2.17	0.95	0.9	1.26		1.37		
SiO <sub>2</sub>	659	816	796	754	931	698	633	670	682		797		
Na	201	188	197	184	128	157	160	246	165		200		
K	32.7	36.5	36.7	31.8	25.7	27.9	24.9	47.2	27.6		34.3		
Ca	0.35	0.28	0.27	0.17	0.23	0.32	0.37	0.72	0.31		0.42		
Mg	0.01	0	0	0	0	0	0	0	0		0.01		
Fe	0.01	0.03	0.01	0.02	0.01	0.01	0	0.02	0.01		0.01		
Al	1.74	1.9	1.68	2.03	2.17	2.01	1.95	1.21	1.93		1.74		
B	1.23	1.36	1.47	1.04	5.92	0.4	0.68	1.01	0.84		1.18		
<i>Steam sample (mmol/kg)</i>													
CO <sub>2</sub>	29.7	52.8	71.8	99.4	55.6	80.9	155.2	9.6	64.8	57.1		36.2	69.8
H <sub>2</sub> S	24.1	33.7	47.1	27.9	27.3	6.2	19.2	3.1	18.1	45.2		14.3	22.7
Ar	0.05	0.13	0.12	0.08	0.03	0.13	0.02	0.01	0.06	0.17		0.01	0.04
N <sub>2</sub>	2.74	8.74	9.44	5.80	1.22	7.5	1.36	0.82	4.19	14.1		0.66	2.61
CH <sub>4</sub>	0.21	0.3	0.26	0.3	0.15	0.56	0.18	0.05	0.38	0.05		0.09	0.2
O <sub>2</sub>	0	0	0	0	0	0	0	0	0	0.86		0	0
H <sub>2</sub>	10.8	21.4	31.0	18.1	14.9	0.51	11.49	0.55	10.3	27.7		6.87	14.83

<sup>a</sup> ReInjection waste water.

volatile components in the discharge are taken to be present in the steam only we have

$$m_s^{f,t} = \frac{M^{d,t}}{M^{f,t}} m_s^{d,t} = \frac{1}{V^{f,t}} m_s^{d,t} \quad (8)$$

since by definition  $V^{f,t} = M^{f,t}/M^{d,t}$ .

Detailed descriptions of the models for calculations of aquifer fluid composition are given by Arnórsson et al. (2007). The aquifer fluid composition was calculated with the aid of the WATCH program version 2.1 (Bjarnason, 1994). In this program  $M_s^{f,t}$  is corrected for gases dissolved in the water retained in the aquifer at  $T^e$ .

### 3.3. Aqueous speciation, mineral saturation state and reaction path modelling

Geochemical model calculations were carried out to gain insight into H<sub>2</sub>S–water–rock interaction under geothermal conditions. This involved calculation of aquifer speciation and mineral saturation states and reaction path modelling. The calculations were carried out using the WATCH (Bjarnason, 1994) and PHREEQC (Parkhurst and Appelo, 1999) programs with appropriated updates of the thermodynamic data sets for aqueous species, gas and mineral solubilities.

The solubility of H<sub>2</sub>S(g) was selected from Suleimenov and Krupp (1994). For other gases, the values reported by Fernandez-Prini et al. (2003) were used. Moreover, the first ionization constant for H<sub>2</sub>S was updated according to the results of Suleimenov and Seward (1997). The data sets and comparisons with other data can be found in the respective papers.

Secondary mineral solubilities were further updated in the present work. The apparent Gibbs energy of formation ( $\Delta G_{i,j,T,p_{sat}}^{app}$ ) at 0–350 °C and water vapour saturation pressures of key aqueous species and minerals necessary to calculate the mineral solubilities were selected. The key aqueous species in the data set include H<sub>2</sub>O, OH<sup>−</sup>, H<sup>+</sup>, Na<sup>+</sup>, K<sup>+</sup>, Mg<sup>2+</sup>, Ca<sup>2+</sup>, Al(OH)<sub>4</sub><sup>−</sup>, Fe<sup>2+</sup>, Fe(OH)<sub>4</sub><sup>−</sup>, H<sub>4</sub>SiO<sub>4</sub>(aq), Ti(OH)<sub>4</sub>(aq), H<sub>2</sub>S(aq), SO<sub>4</sub><sup>2−</sup>, HCO<sub>3</sub><sup>−</sup>, Cl<sup>−</sup>, F<sup>−</sup> and H<sub>2</sub>(aq). Their Gibbs energy values were selected from Supcrt92 slop07.dat (Johnson et al., 1992), Gunnarsson

and Arnórsson (2000), Benezeth et al. (2001), Ziemiak et al. (1993), Hill (1990), Diakonov et al. (1999) and Marshall and Franck (1981). Values for the apparent Gibbs energy of secondary minerals were selected from the data sets given by Holland and Powell (1998), Robie and Hemingway (1995), Neuhoff (2000), Arnórsson and Stefánsson (1999) and Fridriksson et al. (2001). A summary of the stability constants can be obtained in Stefánsson et al. (2009).

Reaction path modelling was carried out to simulate the interactions of basalt with geothermal waters at 100–300 °C and  $p_{sat}$ . The initial water composition was first calculated by mixing H<sub>2</sub>S with waste water from the Hellisheidi power plant (Table 3, sample 08-3011). This mixture was then allowed to react with basaltic glass as a proxy for basalts according to the dissolution rates reported by Gíslason and Oelkers (2003) and the saturated secondary minerals in each step then allowed to precipitate. The composition of the basaltic glass used for the calculations is given in Table 4 and the secondary minerals incorporated in the calculations are given in Table 5. The initial H<sub>2</sub>S concentrations were 1, 5 and 50 mmol kg<sup>−1</sup> that correspond approximately to the concentration range in the current waste waters injected into the geothermal reservoir, the conditions of the geothermal reservoir today and the planned conditions of the

**Table 4**  
Basaltic glass composition used for the geochemical model calculations (from Oelkers and Gíslason, 2001).

	wt.%
SiO <sub>2</sub>	48.12
TiO <sub>2</sub>	1.56
Al <sub>2</sub> O <sub>3</sub>	14.62
Fe <sub>2</sub> O <sub>3</sub>	1.11
FeO	9.82
MnO	0.19
MgO	9.08
CaO	11.84
Na <sub>2</sub> O	1.97
K <sub>2</sub> O	0.29
P <sub>2</sub> O <sub>5</sub>	0.2

**Table 5**

Minerals included in the geochemical model calculations at 100–300 °C and  $p_{\text{sat}}$ .

Mineral	Symbol	Chemical composition
Basaltic glass	BS	$\text{Si}_{1.000}\text{Ti}_{0.024}\text{Al}_{0.358}\text{Fe}_{0.188}\text{Mg}_{0.281}$ $\text{Ca}_{0.264}\text{Na}_{0.079}\text{K}_{0.008}\text{O}_{3.370}$
Quartz	qtz	$\text{SiO}_2$
Opaline silica	opl	$\text{SiO}_2$
Kaolinite	kaol	$\text{Al}_2\text{Si}_2\text{O}_5(\text{OH})_4$
Celadonite	cel	$\text{KMgAlSi}_4\text{O}_{10}(\text{OH})_2$
Fe-celadonite	cel(Fe)	$\text{KFeAlSi}_4\text{O}_{10}(\text{OH})_2$
Mg–Fe smectite	Mg–Fe smc	$\text{Na}_{0.04}\text{K}_{0.10}\text{Ca}_{0.21}\text{Mg}_{1.44}\text{FeAl}_{1.00}\text{Si}_{3.00}\text{O}_{10}(\text{OH})_2$
Clinocllore	chl	$\text{Mg}_5\text{Al}_2\text{Si}_3\text{O}_{10}(\text{OH})_8$
Daphnite	dap	$\text{Fe}_5\text{Al}_2\text{Si}_3\text{O}_{10}(\text{OH})_8$
Epidote	epi	$\text{Ca}_2\text{Al}_2\text{FeSi}_3\text{O}_{12}(\text{OH})$
Clinozoesite	czo	$\text{Ca}_2\text{Al}_3\text{Si}_3\text{O}_{12}(\text{OH})$
Prehnite	pre	$\text{Ca}_2\text{Al}_2\text{Si}_3\text{O}_{10}(\text{OH})_2$
Grossular	gro	$\text{Ca}_3\text{Al}_2\text{Si}_3\text{O}_{12}$
Wollastonite	wo	$\text{CaSiO}_3$
Low-albite	alb	$\text{NaAlSi}_3\text{O}_8$
Micrókline	mic	$\text{KAlSi}_3\text{O}_8$
Chabasite-Ca	cab(Ca)	$\text{CaAl}_2\text{Si}_4\text{O}_{12} \cdot 6\text{H}_2\text{O}$
Chabasite-Na	cab(Na)	$\text{Na}_2\text{Al}_2\text{Si}_4\text{O}_{12} \cdot 6\text{H}_2\text{O}$
Natrolite	nat	$\text{Na}_2\text{Al}_2\text{Si}_3\text{O}_{10} \cdot 2\text{H}_2\text{O}$
Mesolite	mes	$\text{Ca}_{0.667}\text{Na}_{0.666}\text{Al}_2\text{Si}_3\text{O}_{10} \cdot 2.667\text{H}_2\text{O}$
Scolesite	sco	$\text{CaAl}_2\text{Si}_3\text{O}_{10} \cdot 3\text{H}_2\text{O}$
Thomsonite	thm	$\text{Ca}_2\text{NaAl}_5\text{Si}_5\text{O}_{20} \cdot 6\text{H}_2\text{O}$
Mordenite-Ca	mor(Ca)	$\text{Ca}_{0.5}\text{AlSi}_5\text{O}_{12} \cdot 4\text{H}_2\text{O}$
Mordenite-Na	mor(Na)	$\text{NaAlSi}_5\text{O}_{12} \cdot 3\text{H}_2\text{O}$
Heulandite-Ca	heul(Ca)	$\text{CaAl}_2\text{Si}_7\text{O}_{18} \cdot 6\text{H}_2\text{O}$
Heulandite-Na	heul(Na)	$\text{Na}_2\text{Al}_2\text{Si}_7\text{O}_{18} \cdot 5\text{H}_2\text{O}$
Analsime	anl	$\text{Na}_{0.96}\text{Al}_{0.96}\text{Si}_{2.04}\text{O}_6 \cdot 1.02\text{H}_2\text{O}$
Laumontite	lau	$\text{CaAl}_2\text{Si}_4\text{O}_{12} \cdot 4.5\text{H}_2\text{O}$
Leonhardite	leo	$\text{CaAl}_2\text{Si}_4\text{O}_{12} \cdot 3.5\text{H}_2\text{O}$
Yugawaralite	yug	$\text{CaAl}_2\text{Si}_6\text{O}_{16} \cdot 4\text{H}_2\text{O}$
Clinoptilolite-Ca	clp(Ca)	$\text{Ca}_{1.5}\text{Al}_3\text{Si}_{15}\text{O}_{36} \cdot 12\text{H}_2\text{O}$
Clinoptilolite-Na	clp(Na)	$\text{Na}_3\text{Al}_3\text{Si}_{15}\text{O}_{36} \cdot 12\text{H}_2\text{O}$
Stilbite	stb	$\text{Ca}_2\text{NaAl}_5\text{Si}_{13}\text{O}_{36} \cdot 16\text{H}_2\text{O}$
Wairakite	wai	$\text{CaAl}_2\text{Si}_4\text{O}_{12} \cdot 2\text{H}_2\text{O}$
Calcite	cc	$\text{CaCO}_3(\text{s})$
Magnetite	mt	$\text{Fe}_3\text{O}_4$
Pyrite	py	$\text{FeS}_2$
Pyrrhotite	pyrr	$\text{FeS}$
Sulfur	S	S
Anhydrite	anh	$\text{CaSO}_4$

injection fluids after addition and mixing of  $\text{H}_2\text{S}$ , respectively. The calculations were carried out with the aid of the PHREEQC program (Parkhurst and Appelo, 1999) with the updated thermodynamic data sets of reactions and mineral solubilities to 300 °C at  $p_{\text{sat}}$ .

**4. The geochemistry of  $\text{H}_2\text{S}$  in geothermal systems**

The concentrations of  $\text{H}_2\text{S}$  in aquifer fluids at Hellisheidi are shown in Fig. 1. For comparison the concentrations of  $\text{H}_2$  are also shown. The calculated concentrations of  $\text{H}_2\text{S}$  in the aquifers at the Hellisheidi geothermal system match very well equilibrium assemblages according to the reactions

$$1/3\text{py} + 1/3\text{pyrr} + 2/3\text{pre} + 2/3\text{H}_2\text{O} = 2/3\text{epi} + \text{H}_2\text{S}(\text{aq}) \quad (9)$$

$$1/4\text{py} + 1/2\text{pyrr} + \text{H}_2\text{O} = 1/4\text{mt} + \text{H}_2\text{S}(\text{aq}) \quad (10)$$

For dissolved  $\text{H}_2$  the concentrations are somewhat higher than those corresponding to the same mineral buffer reactions.

$$3/4\text{pyrr} + 2/3\text{pre} + 2/3\text{H}_2\text{O} = 2/3\text{epi} + 2/3\text{py} + \text{H}_2(\text{aq}) \quad (11)$$

$$\text{pyrr} + \text{H}_2\text{O} = 3/4\text{py} + 1/4\text{mt} + \text{H}_2(\text{aq}) \quad (12)$$

For the only liquid enthalpy well (HE-5) included in this study, calculated aquifer fluid  $\text{H}_2\text{S}$  concentrations were somewhat lower

relative to equilibrium, as was the case for the hottest well (HE-29). One excess enthalpy well had quite low aquifer fluid  $\text{H}_2\text{S}$  concentrations (HE-3). The discharge of this well was also low in other gases, indicating that boiled and degassed water enter this well. Other wells had slightly higher aquifer fluid  $\text{H}_2\text{S}$  concentrations than those corresponding to equilibrium with the prehnite bearing assemblage. Magnetic lows are typically found over high temperature areas in Iceland (Pálmason, 1975), indicating that magnetite is unstable. Therefore, it is considered that the mineral assemblage with which  $\text{H}_2\text{S}$  tends to equilibrate is the prehnite containing one. For  $\text{H}_2$ , the results were more exaggerated than those for  $\text{H}_2\text{S}$ , i.e. the data points were further above and below the equilibrium curve, though the systematic was the same.

Hydrogen sulphide is more soluble in water than  $\text{H}_2$ . This explains the observed pattern of the data points in Fig. 1. Two well discharges were degassed (HE-03 and HE-05) and more degassed for  $\text{H}_2$  than  $\text{H}_2\text{S}$  because of the lower solubility in water of the former. The discharge of the remaining wells contained some excess initial aquifer steam. This initial or gas equilibrium aquifer steam fraction may be estimated assuming local mineral equilibria with respect to reactions (9) and (11) according to the expression

$$x^{f,v} = \frac{A_{\text{H}_2\text{S}} - A_{\text{H}_2}}{\frac{55.51}{p_{\text{total}}} \left( \frac{A_{\text{H}_2}}{K_{\text{H}_2\text{S}}} - \frac{A_{\text{H}_2\text{S}}}{K_{\text{H}_2}} \right) + A_{\text{H}_2\text{S}} - A_{\text{H}_2}} \quad (13)$$

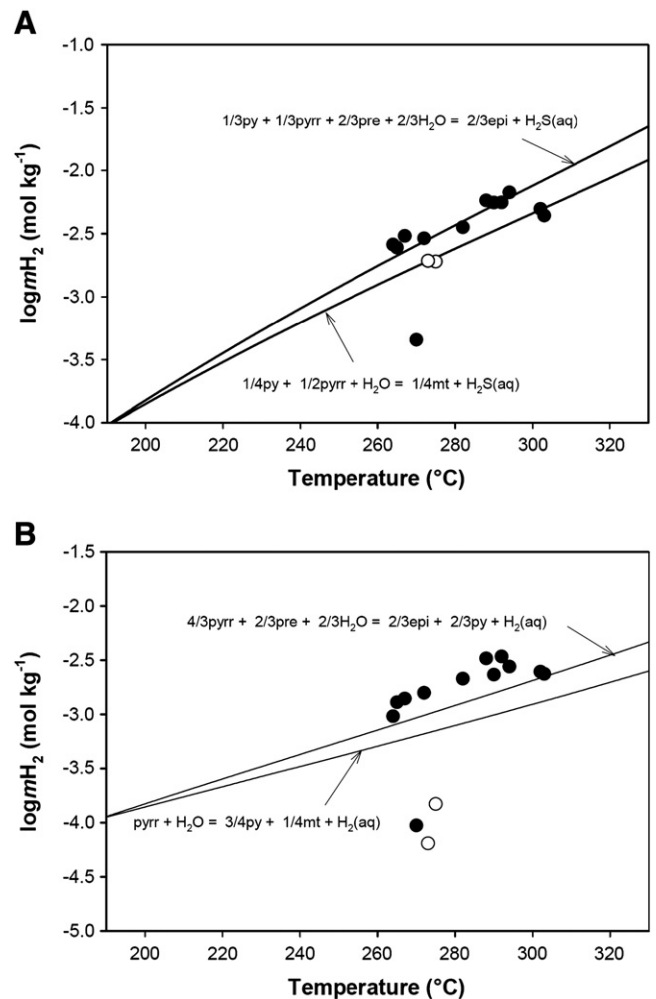


**Fig. 1.** The concentration of aquifer  $\text{H}_2\text{S}$  and  $\text{H}_2$  in geothermal fluids at Hellisheidi. Open symbols represent liquid enthalpy well discharges and filled symbols excess enthalpy well discharges. The curves represent equilibrium concentration according to the respective reactions.

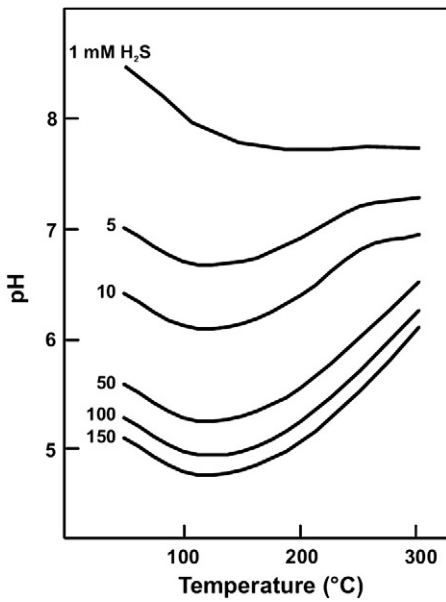


Fig. 2. The effects on pH of H<sub>2</sub>S addition to wastewater as a function of temperature at the Hellisheidi geothermal field, SW Iceland.

where  $A_{H_2} m_{H_2}^{d,t} / m_{H_2}^{f,l}$ ,  $A_{H_2S} = m_{H_2S}^{d,t} / m_{H_2S}^{f,l}$  and  $K_{H_2S}$  and  $K_{H_2}$  are the H<sub>2</sub>S and H<sub>2</sub> solubility constants in water, respectively (see Arnórsson et al., 2007). The H<sub>2</sub>S and H<sub>2</sub> concentrations in the discharge are

known ( $m_s^{d,t}$ ). The gas concentrations in the aquifer liquid can be calculated from the equilibrium constants of the mineral buffer reactions ( $m_s^{f,l}$ ). The estimated aquifer steam fraction according to these calculations at Hellisheidi was negligible (<0.5% by weight of the aquifer fluid) but enough to cause an increase in H<sub>2</sub> in the well discharge. It should be pointed out that similar calculations for other geothermal systems in Iceland like Nesjavellir and Krafla often indicate a significant aquifer steam fraction, of tens of percentage points by volume (Arnórsson et al., 2007).

5. H<sub>2</sub>S–water–basalt interaction under geothermal conditions

The geochemical aspects of the effects of H<sub>2</sub>S injection into the Hellisheidi geothermal system can be divided into two parts, firstly

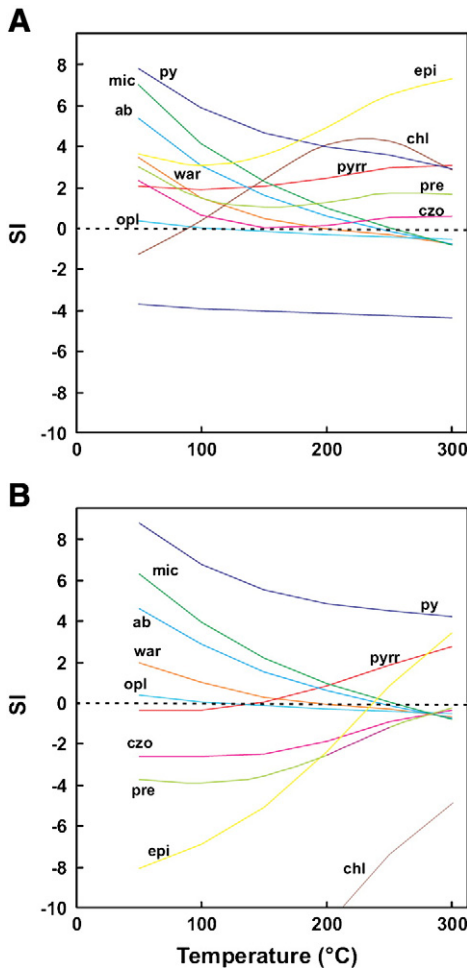


Fig. 3. Mineral saturation in injection waters at the Hellisheidi geothermal field, SW Iceland. A) Current injection fluids and B) in injection fluids containing 50 mmol kg<sup>-1</sup> H<sub>2</sub>S.

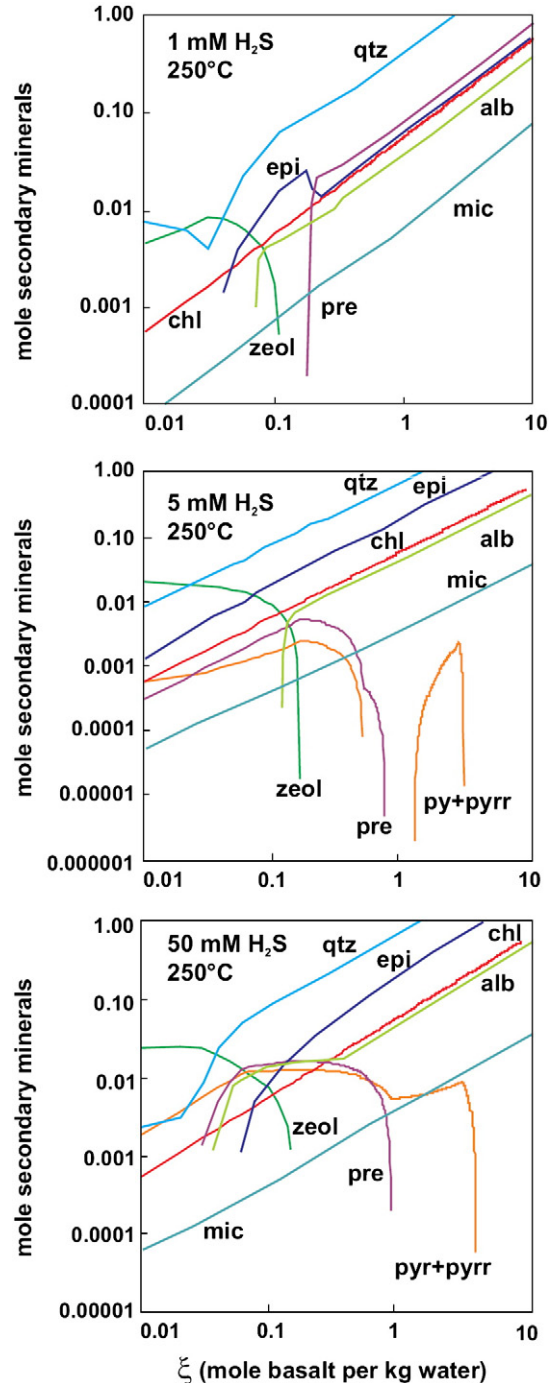


Fig. 4. The effects of addition of H<sub>2</sub>S on secondary mineral formation at 250 °C.

the effects on addition of H<sub>2</sub>S to the wastewater injected at present and secondly the reactions between H<sub>2</sub>S-charged injection waters with the basaltic rocks under geothermal conditions.

The wastewater injected at present into the Hellisheidi geothermal system (Table 3, 08-3011) is a typical low salinity boiling high-temperature geothermal water. The water pH is alkaline, the dissolved gas concentrations are low and the silica concentrations high.

The total emission of H<sub>2</sub>S from the Hellisheidi power plant is 12,950 tonnes yr<sup>-1</sup> and total injection into the geothermal system is 305 kg s<sup>-1</sup>, assuming all H<sub>2</sub>S to be mixed with the injection water corresponding to about 1300 ppm (~40 mmol kg<sup>-1</sup>) H<sub>2</sub>S in the injection water after mixing. The natural H<sub>2</sub>S aquifer concentrations are between 15 and 228 ppm with an average value of 130 ppm (~4 mmol kg<sup>-1</sup>). Injection of H<sub>2</sub>S charged water into the reservoir would therefore increase the H<sub>2</sub>S concentration about ten times.

The addition of H<sub>2</sub>S to the injected water influenced primarily two things, the H<sub>2</sub>S concentration and its pH value. The pH of the H<sub>2</sub>S wastewater mixtures are shown in Fig. 2 as a function of temperature and H<sub>2</sub>S concentration. The pH was lowered relatively rapidly by the addition of H<sub>2</sub>S. At H<sub>2</sub>S concentrations below 10 mmol kg<sup>-1</sup>, the pH was buffered primarily by the ionization of silica as well as a small contribution of added H<sub>2</sub>S. However, for solutions with H<sub>2</sub>S concentrations exceeding 50 mmol kg<sup>-1</sup> the pH was predominantly buffered by the ionization of H<sub>2</sub>S to form HS<sup>-</sup>.

The addition of H<sub>2</sub>S to the wastewater and the accompanying decrease in pH had some significant effects on the mineral saturation state (Fig. 3). Many common geothermal minerals are observed to be supersaturated with the possibility of scaling formation during injection. In particular, silica polymerization and scaling are often

observed to be the main problem. The addition of H<sub>2</sub>S resulted in undersaturation with respect to many aluminium silicates like clays, epidote and prehnite, but supersaturation with respect to sulphides. However, it has insignificant effects on silica saturation, but may none the less lower silica polymerization rates as these are pH dependent (Gunnarsson and Arnórsson, 2008). Hydrogen sulphide addition, or in fact any other weak acid addition, may decrease scaling potential during injection of wastewater into high temperature geothermal systems.

To identify the effects of H<sub>2</sub>S on geothermal alteration of basalt, sets of reaction path model calculations were carried out. The composition of the basaltic glass and secondary minerals allowed are listed in Tables 4 and 5.

Upon addition of 5–50 mmol H<sub>2</sub>S, for a system that had reacted with about 0.1 to 1 mol of basalt (ca 10–100 g basalt) per kg of water, quartz or chalcedony and sulphides were observed to form at all temperatures between 100 and 300 °C (Fig. 4). This is in good agreement with observations from active and fossil geothermal systems hosted by basaltic rocks. Smectites, generally containing Fe, Mg, J and Ca, were calculated to be stable at temperatures below 150 °C, whereas they were replaced by chlorite and epidote, and by prehnite as well for a restricted reaction progress range, at about 200–230 °C. The addition of H<sub>2</sub>S to the geothermal fluids did not change the overall secondary mineralogy to a large extent. The main differences were abundant sulphide formations and possibly elemental sulphur formation below 150 °C as well as formation of simple hydroxides and aluminium silicates like kaolinite that are often observed under acid conditions.

The results of the calculations showed that for a two phase (solid and liquid) closed system at local equilibrium three factors controlled

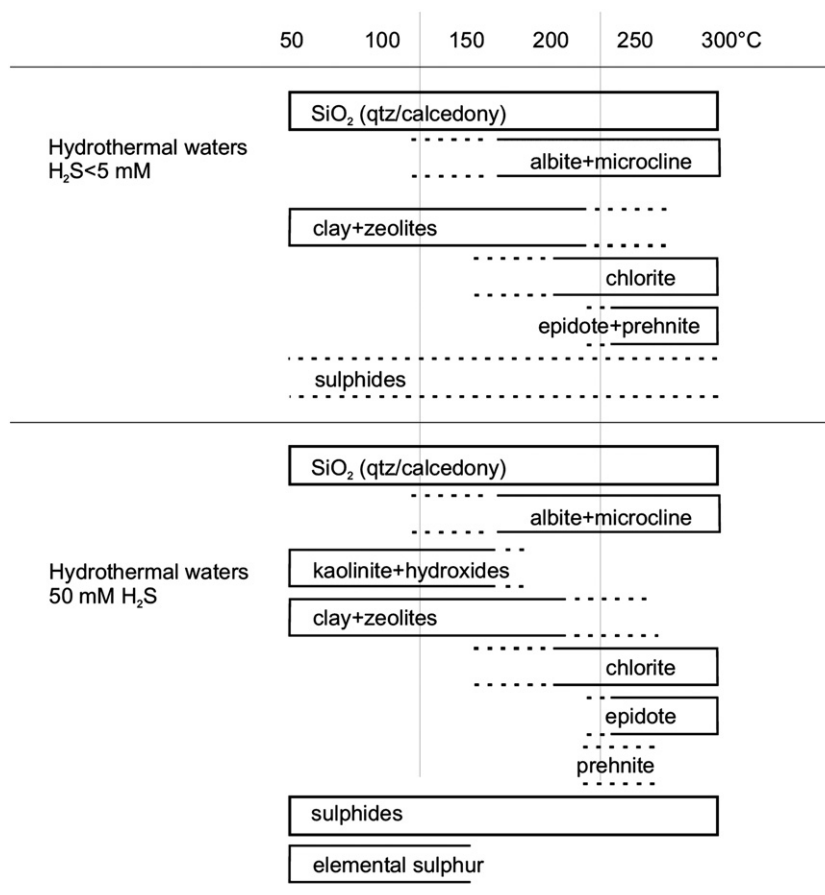


Fig. 5. Predominant secondary mineral formation at a constant water–rock ratio (approximately 10–100 g basalt per 1 kg water) as a function of temperature at low and elevated H<sub>2</sub>S concentrations.

the water–rock interaction and the respective fluid chemistry and secondary mineralogy (Fig. 5): firstly, acid supply shifting mineral stabilities, cation availability and quantity of acid ( $\text{H}_2\text{S}$ ) to be mineralized, secondly, the temperature affecting mineral stability and cation availability, and thirdly the extent of reaction that affected the relative concentration of dissolved solids and secondary minerals. It is possible that the system attained a steady state between acid supply and consumption of acids ( $\text{H}^+$ ) by the primary basaltic glass and secondary minerals that in turn were affected by both the solution pH and degree of basalt dissolution. The important thing is that at a specific temperature, the system underwent changes in predominant secondary mineral assemblages as a function of the extent of the reaction. For example, at 250 °C, zeolites predominated at a low reaction progress and were replaced by epidote and prehnite with increasing glass dissolution, whereas the formation of alkali feldspars, quartz and chlorite seems to have been more or less independent of reaction progress. The addition of  $\text{H}_2\text{S}$ , changed the reaction pattern with sulphides becoming more important geothermal minerals as well as affecting the fine details of the formation of Ca-rich minerals like zeolites, prehnite and epidote that take part in the mineral buffer reactions for  $\text{H}_2\text{S}$ . Minerals that are not included in the  $\text{H}_2\text{S}$  mineral-buffer reactions were more or less unaffected, like quartz, alkali feldspars and chlorite.

The quantity and rate of sulphide mineralization was mostly affected by the availability and oxidation state of iron. At low pH values  $\text{Fe}^{2+}$  predominated. With increasing pH and temperature, hydrolysis produced more  $\text{Fe}(\text{OH})_3(\text{aq})$ , and  $\text{Fe}(\text{OH})_4^-$  became the dominant iron species, thus reducing the availability of  $\text{Fe}^{2+}$  for pyrite formation. In addition, competition of secondary mineral for iron, mainly smectites at <150 °C and epidote at >230 °C, reduced the availability of iron for sulphide formation. This is clearly reflected in the amount of basaltic glass dissolution needed to mineralize  $\text{H}_2\text{S}$  (Fig. 6). The amount of basalt needed to mineralize and initial 50 mmol  $\text{kg}^{-1}$   $\text{H}_2\text{S}$  down to the equilibrium concentrations at 200 °C was about 1 mol, whereas at 300 °C more than 1 mol of basalt was needed, yet the equilibrium concentrations at 200 °C were two orders of magnitude lower than at 300 °C. The reason is that at 300 °C almost all the iron dissolved from the basalt went into epidote. Based on the above, the optimized reservoir conditions for  $\text{H}_2\text{S}$  injection can be selected. The aim is that the  $\text{H}_2\text{S}$  will be mineralized and diluted upon entering the geothermal aquifer before it enters the producing wells. To maximize  $\text{H}_2\text{S}$  mineralization capacity, injection into aquifers with temperatures below ~230 °C is favoured, i.e. below the stability of epidote (Fig. 6).

The mass of basaltic glass needed to mineralize  $\text{H}_2\text{S}$  was estimated based on the results of the reaction path modelling. The quantity of basalt needed, assuming all iron dissolved to enter pyrite, was further calculated for comparison. The results are shown in Table 6. As clearly seen, considerable basalt dissolution is needed to sequester  $\text{H}_2\text{S}$  from the Hellisheidi power plant per year; however, the results are very much dependent on the proportion of dissolved iron that goes into pyrite formation.

Oxidation of  $\text{H}_2\text{S}$  to sulphuric acid is among the main concerns when large quantities of  $\text{H}_2\text{S}$  are injected into the Hellisheidi geothermal system. Hydrogen sulphide is a weak acid and in concentrated  $\text{H}_2\text{S}$  solutions at >200 °C the pH does not usually go below 5. On the other hand,  $\text{H}_2\text{SO}_4$ , is a strong acid and in concentrated solutions at >200 °C the pH may even reach values below 2. Such low pH values will in turn greatly enhance rock leaching, metal mobility and corrosion problems. Geothermal fluids are reduced with measurable concentrations of  $\text{H}_2$  commonly in the range 0.01 to 0.1 bar (Stefánsson and Arnórsson, 2002). Under such reduced conditions,  $\text{H}_2\text{S}$  is thermodynamically stable. However, the oxidation mechanism of  $\text{H}_2\text{S}$  under reduced geothermal conditions has not been well studied, including the effects of water pH, metal redox reactions and metal surfaces during injection and in the

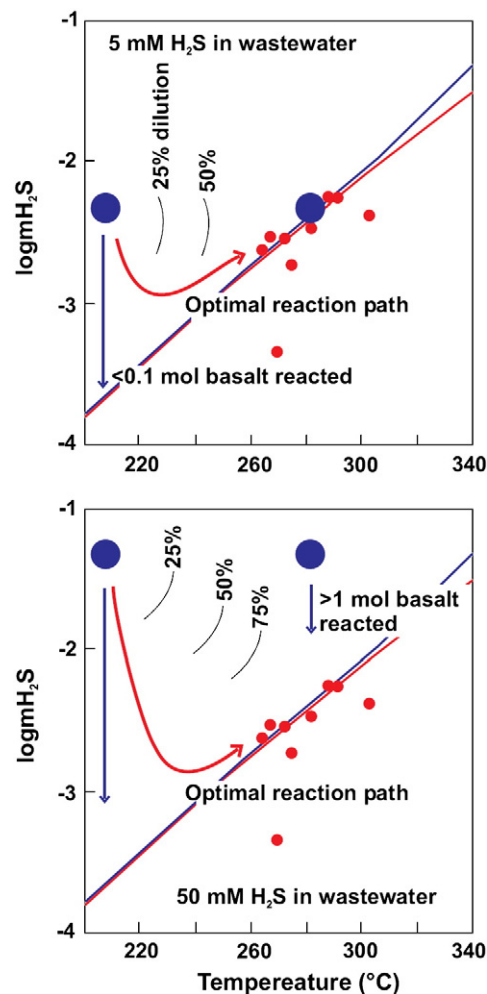


Fig. 6.  $\text{H}_2\text{S}$  geochemistry in the Hellisheidi geothermal system and mass transfer and mixing upon injection of wastewater. At temperatures <220 °C considerably less basalt is needed (horizontal arrows) for  $\text{H}_2\text{S}$  mineralization compared to >250 °C. This is related to iron mobility that is greatly reduced upon epidote formation at >230 °C. The optimized reaction and mixing path would be injection with considerable mineralization at <230 °C followed by mixing of aquifer fluids.

geothermal system itself. To qualitatively assess the effects of  $\text{H}_2\text{S}$  oxidation the fluids were oxides injected in steps and the respective fluid composition calculated. The results are shown in Fig. 7. The results indicate that a considerable fraction of  $\text{H}_2\text{S}$  needs to be oxidised to reach a pH value below 4, with the exact quantity depending on the  $\text{H}_2\text{S}$  concentration in the injection fluid. The example and lack of detailed understanding of  $\text{H}_2\text{S}$  oxidation in geothermal waters clearly demonstrate that full caution and sufficient monitoring is needed.

The reaction progress modelling can be linked to reaction time, given that the rates of reactions are known as well as the mineral

Table 6  
The quantity of basalt needed to sequester  $\text{H}_2\text{S}$  at 250 °C.

$\text{H}_2\text{S}$ in injection fluids (mmol $\text{kg}^{-1}$ )	Geochemical model <sup>a</sup> (tonnes $\text{yr}^{-1}$ basalt)	All Fe into sulfides <sup>b</sup>	Geochemical model <sup>a</sup> ( $\text{m}^3 \text{yr}^{-1}$ basalt <sup>c</sup> )	All Fe into sulfides <sup>b</sup>
5	2950	126	1020	43
50	926	126	320	43

<sup>a</sup> Rate of  $\text{H}_2\text{S}$  mineralization according to the geochemical models.

<sup>b</sup> Rate of  $\text{H}_2\text{S}$  mineralization assuming all Fe from the basalt to go into pyrite formation.

<sup>c</sup> Density of basalt 2.9.

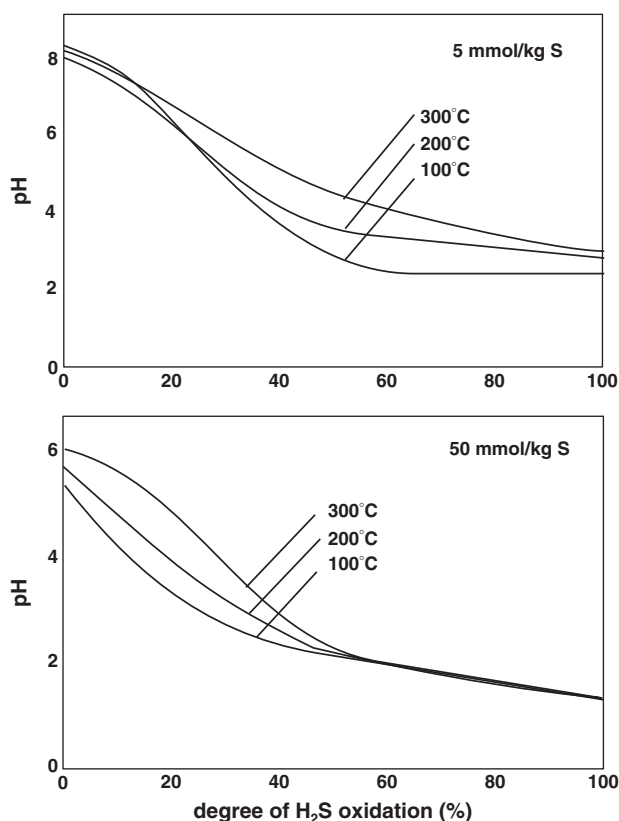


Fig. 7. The relationship between calculated pH and degree of H<sub>2</sub>S oxidation at 100, 200 and 300 °C.

reactive surface areas. In the present study the dissolution rate of the primary rocks was assumed to be that for basaltic glass as determined by Gíslason and Oelkers (2003) using a reactive surface area of 250 cm<sup>2</sup>/g. However, there are four basic problems associated with calculations of the time dependence of the progress of the reaction. It is well known that the estimation of the true reactive surface area is difficult, as well as the effects of surface roughness, porosity and secondary mineral coatings (e.g. White and Brantley, 2003) and for the Hellisheidi system the reactive surface area is simply unknown. In addition, as demonstrated by Gysi and Stefánsson (2011a, 2011b) it may be very difficult to calculate accurately the mass movement as a function of time for well constrained batch systems and within the uncertainties of the reactive mineral surface areas time differences of the up to 2 to 5 fold can be easily observed. Another fundamental problem is related to the dissolution mechanism and rock crystallinity. The approach used in the present study was to assume stoichiometric dissolution of bulk basalt and quantify the dissolution rate as it approached equilibrium by the chemical affinity of a Si–Al leached layer (Oelkers and Gíslason, 2001). This may not be the true case, however, as the rocks contain primary minerals like olivine, plagioclase and pyroxene in addition to basaltic glass. In addition, most dissolution rate experiments of basaltic glass have been conducted at low temperatures far from equilibrium (e.g. Daux et al., 1997; Wolff-Boenisch et al., 2004a, 2004b; Flaathen et al., 2010) and the dissolution mechanism at high-temperatures may differ. Because of these uncertainties we concluded that accurate time dependence of the reaction progress at Hellisheidi was speculative, though, because of the high temperatures (<250 °C), most likely relatively rapid.

## 6. Summary and conclusions

Reykjavík Energy, Iceland, is currently planning to sequester H<sub>2</sub>S into boreholes in the Hellisheidi geothermal system, where the

geothermal gases (CO<sub>2</sub>, H<sub>2</sub>S, H<sub>2</sub> and N<sub>2</sub>) will be separated in a gas abatement station and the H<sub>2</sub>S stream mixed at the surface with wastewater from steam separators and condensed steam and subsequently injected into >230 °C geothermal aquifers where the H<sub>2</sub>S will be mineralized. Considerable geochemical uncertainties are related to the injection of H<sub>2</sub>S, including the effects of the H<sub>2</sub>S supply on fluid–rock interaction and rate and mechanism of H<sub>2</sub>S mineralization. In order to evaluate these uncertainties the geochemistry of H<sub>2</sub>S was studied under aquifer conditions at Hellisheidi.

The results indicate that the concentration of H<sub>2</sub>S in the initial aquifer fluids is in the range of 15 to 228 ppm with an average value of 130 ppm. The concentration is controlled by local equilibrium with pyrite, pyrrhotite, prehnite and epidote when temperatures are above 230 °C.

Injection of H<sub>2</sub>S will significantly increase the reservoir H<sub>2</sub>S equilibrium concentrations. This will result in mineralization of pyrite and possibly other sulphides as well. Based on reaction modelling, the main factor affecting the H<sub>2</sub>S mineralization capacity is related to the mobility and oxidation of iron. At low pH values, Fe<sup>2+</sup> is the predominant iron species whereas with increasing pH and temperature, hydrolysis makes Fe(OH)<sub>3</sub>(aq) and Fe(OH)<sub>4</sub><sup>-</sup> more important. In addition, smectites at <150 °C and epidote at >230 °C greatly reduce the availability of iron for pyrite formation, leading to the need for a much greater basaltic glass dissolution to sequester the H<sub>2</sub>S injected into the system. Based on these findings, the optimum conditions of H<sub>2</sub>S injections are into aquifers with temperatures below 230 °C where epidote is unstable. Upon mineralization, dilution, heating of the injected water and its mixing with aquifer fluids, it is anticipated that injected H<sub>2</sub>S will be sequestered. Injection into much hotter aquifers would result in the need for much greater mass movement (basaltic glass dissolution) for H<sub>2</sub>S mineralization as most of the iron dissolved is expected to enter epidote.

## Acknowledgements

We would like to thank G. Chiodini for editorial handling and L. Marini and an anonymous reviewer for their reviews that greatly improved the present contribution. This research project was funded by Reykjavík Energy.

## References

- Arnórsson, S., 1995a. Geothermal systems in Iceland: structure and conceptual models: 1. High-temperature areas. *Geothermics* 24, 561–602.
- Arnórsson, S., 1995b. Geothermal systems in Iceland: structure and conceptual models: 2. Low-temperature areas. *Geothermics* 24, 603–629.
- Arnórsson, S., Bjarnason, J.Ö., Giroud, N., Gunnarsson, I., Stefánsson, A., 2006. Sampling and analysis of geothermal fluids. *Geofluids* 6, 203–216.
- Arnórsson, S., Gunnlaugsson, E., Svavarsson, H., 1983. The chemistry of geothermal waters in Iceland: 2. Mineral equilibria and independent variables controlling water compositions. *Geochim. Cosmochim. Acta* 47, 547–566.
- Arnórsson, S., Stefánsson, A., 1999. Assessment of feldspar solubility constants in water in the range 0° to 350 °C at vapour saturation pressures. *Am. J. Sci.* 299, 173–209.
- Arnórsson, S., Stefánsson, A., Bjarnason, J.Ö., 2007. Fluid–fluid interaction in geothermal systems. In *Rev. Min. Geochem.* 65, 259–312.
- Benezeth, P., Palmer, D.A., Wesolowski, D.J., 2001. Aqueous high-temperature solubility studies: II. The solubility of boehmite at 0.03 m ionic strength as a function of temperature and pH as determined by in situ measurements. *Geochim. Cosmochim. Acta* 65, 2097–2111.
- Bjarnason, J.Ö., 1994. The speciation program WATCH version 2.1A. Icelandic National Energy Authority Report <http://www.geothermal.is/software/software>.
- Crandell, L.E., Ellis, B.R., Peters, C.A., 2010. Dissolution potential of SO<sub>2</sub> co-injection with CO<sub>2</sub> in geological sequestration. *Environ. Sci. Technol.* 44, 349–355.
- Daux, V., Guy, C., Advocat, T., Crovisier, J.L., Stille, P., 1997. Kinetic aspects of basaltic glass dissolution at 90 °C: role of aqueous silicon and aluminium. *Chem. Geol.* 142, 109–126.
- Diakonov, I., Schott, J., Martin, F., Harrichourry, J.-C., Escalier, J., 1999. Iron (III) solubility and speciation in aqueous solutions: experimental study and modelling: part 1. Hematite solubility from 60 to 300 °C in NaOH–NaCl solutions and thermodynamic properties of Fe(OH)<sub>4</sub><sup>-</sup>(aq). *Geochim. Cosmochim. Acta* 63, 2247–2261 491.
- Fernandez-Prini, R., Alvarez, J.L., Harvey, A.H., 2003. Henry's constants and vapor–liquid distribution constants for gaseous solutes in H<sub>2</sub>O and D<sub>2</sub>O at high temperatures. *J. Phys. Chem. Ref. Data* 32, 903–916.

- Flaathen, T.K., Gíslason, S.R., Oelkers, E.H., 2010. The effect of aqueous sulphate on basaltic glass dissolution rates. *Chem. Geol.* 277, 345–454.
- Foulger, G.R., 1988. Hengill triple junction, SW Iceland: 2. Anomalous earthquake focal mechanisms and implications for process within the geothermal reservoir and at accretionary plate boundaries. *J. Geophys. Res.* 93, 13,507–13,523.
- Fridleifsson, G.O., 1991. Geothermal systems and associated alteration in Iceland. *Geol. Surv. Jpn. Rep.* 277, 83–90.
- Fridriksson, T., Neuhoﬀ, P.S., Arnórsson, S., Bird, D.K., 2001. Geological constraints on the thermodynamic properties of the stilbite–stellerite solid solution in low-grade metabasalts. *Geochim. Cosmochim. Acta* 65, 3993–4008.
- Gessner, K., Kuhn, M., Rath, V., Kosack, C., Blumenthal, M., Clauser, C., 2009. Coupled process models as a tool for analyzing geothermal systems. *Surv. Geophys.* 30, 133–162.
- Giggenbach, W.F., 1980. Geothermal gas equilibria. *Geochim. Cosmochim. Acta* 44, 2021–2032.
- Giggenbach, W.F., 1981. Geothermal mineral equilibria. *Geochim. Cosmochim. Acta* 45, 393–410.
- Gíslason, S.R., Oelkers, E.H., 2003. Mechanism, rates, and consequences of basaltic glass dissolution: II. An experimental study of the dissolution rates of basaltic glass as a function of pH and temperature. *Geochim. Cosmochim. Acta* 67, 3817–3832.
- Gíslason, S.R., Wolff-Boenisch, D., Stefánsson, A., Oelkers, E.H., Gunnlaugsson, E., Sigurdardóttir, H., Sigfusson, B., Broecker, W.S., Matter, J.M., Stute, M., Axelsson, G., Fridriksson, Th., 2010. Mineral sequestration of carbon dioxide in basalt: a preinjection overview of the CarbFix project. *Int. J. Greenhouse Gas Control* 4, 537–545.
- Gudmundsson, B.T., Arnórsson, S., 2005. Secondary mienarl–fluid equilibria in the Krafla and Námafjall geothermal systems. *Iceland. Appl. Geochem.* 20, 1607–1625.
- Gunnarsson, I., Arnórsson, S., 2000. Amorphous silica solubility and the thermodynamic properties of  $H_4SiO_4$  in the range of 0° to 350 °C at Psat. *Geochim. Cosmochim. Acta* 64, 2295–2307.
- Gunnarsson, I., Arnórsson, S., 2008. Impact of silica scaling on the efficiency of heat extraction from high-temperature geothermal fluids. *Geothermics* 84, 820–829.
- Gunter, W.D., Perkins, E.H., Hutcheon, I., 2000. Aquifer disposal of acid gases: modeling of water–rock reactions for trapping of acid wastes. *Appl. Geochem.* 15, 1085–1095.
- Gysi, A.P., Stefánsson, A., 2011a.  $CO_2$ –water–basalt interaction: I. Low-temperature experiments and implications for  $CO_2$  sequestration into basalts. *Geochim. Cosmochim. Acta* (submitted).
- Gysi, A.P., Stefánsson, A., 2011b.  $CO_2$ –water–basalt interaction: II. Low-temperature reaction path modelling and comparison with experimental and natural data. *Geochim. Cosmochim. Acta* (submitted).
- Hill, P.G., 1990. A unified fundamental equation for the thermodynamic properties of  $H_2O$ . *J. Phys. Chem. Ref. Data* 19, 1233–1274.
- Holland, T.J.B., Powell, R., 1998. An internally consistent thermodynamic data set for phases of petrologic interest. *J. Metamorph. Petrol.* 16, 309–343.
- Hreggvidsdóttir, H., 1987. The green schist to amphibolite facies transition in the Nesjavellir geothermal system, Southwest Iceland. M.Sc. thesis, Univ. Stanford, 66 pp.
- Jacquemet, N., Pironon, J., Saint-Marc, J., 2008. Mineralogical changes of a well cement in various  $H_2S$ – $CO_2$ –brine fluids at high pressure and temperature. *Environ. Sci. Technol.* 42, 282–288.
- Johnson, J.W., Nitao, J.J., Steefel, C.I., Knauss, K.G., 2001. Reactive transport modeling of geological  $CO_2$  sequestration in saline aquifers: the influence of intra-aquifer shales and the relative effectiveness of structural, solubility, and mineral trapping during prograde and retrograde sequestration. In *Proc. First Nat'l Conf. Carbon Sequestration*, Nat. Energy Tech. Lab., Washington DC.
- Johnson, J.W., Oelkers, E.H., Helgeson, H.C., 1992. SUPCRT92. A software package for calculating the standard molal thermodynamic properties of minerals, gases, aqueous species, and reactions from 1 to 5000 bar and 0 to 1000 °C. *Comput. Geosci.* 18, 899–947.
- Knauss, K.G., Johnson, J.W., Steefel, C.I., 2005. Evaluation of the impact of  $CO_2$ , co-contaminant gas, aqueous fluid and reservoir rock interactions on the geologic sequestration of  $CO_2$ . *Chem. Geol.* 217, 339–350.
- Kristmannsdóttir, H., 1979. Alteration of basaltic rocks by geothermal 547 activity at 100–300 °C. In: Mortland, M., Farmer, V. (Eds.), *Developments in Sedimentology*. Elsevier, Amsterdam, pp. 359–367.
- Larsson, D., Grönvald, K., Óskarsson, N., Gunnlaugsson, E., 2002. Geothermal alteration of plagioclase and growth of secondary feldspar in the Hengill volcanic centre, SW Iceland. *J. Volcanol. Geoth. Res.* 114, 275–290.
- Marshall, W.L., Franck, E.U., 1981. Ion product of water substance 0°–1000 °C, 1–10, 000 bar. New international formulation and its background. *J. Phys. Chem. Ref. Data* 10, 295–304.
- Matter, J.M., Broecker, W.S., Stute, M., Gíslason, S.R., Oelkers, E.H., Stefánsson, A., Wolff-Boenisch, D., Gunnlaugsson, E., Axelsson, G., Björnsson, G., 2009. Permanent carbon dioxide storage into basalts: the CarbFix pilot project, Iceland. *Energy Procedia* 1, 3641–3646.
- McPherson, B.J.O.L., Lichtner, P.C., 2001.  $CO_2$  sequestration in deep aquifers. In *Proc. First National Conf. Carbon Sequestration*, Nat. Energy Tech. Lab., Washington DC.
- Neuhoff, P.S., 2000. Thermodynamic properties and parageneses of rock-forming zeolites. Ph.D. Thesis, Stanford University, Stanford, CA, 240 pp.
- Oelkers, E.H., Gíslason, S.R., 2001. Mechanism, rates, and consequences of basaltic glass dissolution: I. An experimental study of the dissolution rates of basaltic glass as a function of aqueous Al, Si and oxalic acid concentrations. *Geochim. Cosmochim. Acta* 65, 3671–3681.
- Palandri, J.L., Kharaka, Y.K., 2008. Ferric iron-bearing sediments as a mineral trap for  $CO_2$  sequestration: iron reduction using sulphur-bearing waste gas. *Chem. Geol.* 217, 351–364.
- Parkhurst, D.L., Appelo, C.A.J., 1999. User's guide to PHREEQC (Version 2)—a computer program for speciation, batch-reaction, one-dimensional transport, and inverse geochemical calculations. U.S. Geological Survey Water-Resources Investigations Report, pp. 99–4259. 310 pp.
- Robie, R.A., Hemingway, B.S., 1995. Thermodynamic properties of minerals and related substances at 298.15 K and 1 bar (105 Pascals) pressure and higher temperatures. *US Geol. Surv. Bull.* 1452 436 pp.
- Sæmundsson, K., 1967. Vulkanismus und tektonik des Hengill gebietes in Sudwest Island. *Acta Nat. Isl.* 2, 1–109 (In German).
- Sæmundsson, K., 1992. Geology of the Thingvallavatn area. *Oikos* 64, 40–68.
- Sanopoulos, D., Karabelas, A., 1997.  $H_2S$  abatement in geothermal plants: evaluation of process alternatives. *Energy Resour.* 19, 63–77.
- Schiffman, P., Fridleifsson, G.O., 1991. The smectite–chlorite transition in drillhole NH-15 Nesjavellir geothermal field, Iceland: XRD, BSE and electron microscope investigations. *J. Metamorph. Geol.* 9, 679–696.
- Sigmundsson, F., Einarsson, P., Rognvaldsson, S.Th., Foulger, G.R., Hodekinsson, K.M., Thorbergsson, G., 1997. The 1994–1995 seismicity and deformation at the Hengill triple junction, Iceland: triggering of earthquakes by minor magma injection in a zone of horizontal shear stress. *J. Geophys. Res.* 102, 15,151–15,161.
- Stefánsson, A., Arnórsson, S., Gunnarsson, I., Kaasalainen, H., 2009. Sequestration of  $H_2S$  from the Hellisheidi power plant – a geochemical study. *Sci. Inst. Report RH-14-2009*. 84 pp.
- Stefánsson, A., Gunnarsson, I., Giroud, N., 2007. New methods for the direct determination of dissolved inorganic, organic and total carbon in natural waters by Reagent-Free™ ion chromatography and inductively coupled plasma atomic emission spectrometry. *Anal. Chim. Acta* 582, 69–74.
- Stefánsson, S., Arnórsson, S., 2000. Feldspar saturation state in natural waters. *Geochim. Cosmochim. Acta* 64, 2567–2584.
- Stefánsson, A., Arnórsson, S., 2002. Gas pressures and redox reactions in geothermal systems in Iceland. *Chem. Geol.* 190, 251–271.
- Suleimenov, O.M., Krupp, R.E., 1994. Solubility of hydrogen sulphide in pure water and in NaCl solutions from 20 to 320 °C and at saturation pressures. *Geochim. Cosmochim. Acta* 58, 2433–2444.
- Suleimenov, O.M., Seward, T.M., 1997. A spectrophotometric study of hydrogen sulphide ionisation in aqueous solutions to 350 °C. *Geochim. Cosmochim. Acta* 61, 5187–5198.
- White, A.F., Brantley, S.L., 2003. The effect of time on the weathering of silicate minerals: why do weathering rates differ in the laboratory and field. *Chem. Geol.* 202, 479–506.
- White, S.P., Allis, R.G., Moore, J., Chidsey, T., Morgan, C., Gwynn, W., 604 Adams, M., 2005. Simulation of reactive transport of injected  $CO_2$  in the Colorado Plateau, Utah, USA. *Chem. Geol.* 217, 387–405.
- Wolff-Boenisch, D., Gíslason, S.R., Oelkers, E.H., 2004a. The effect of fluoride on the dissolution rates of natural glasses at pH 4 and 25 °C. *Geochim. Cosmochim. Acta* 68, 4571–4582.
- Wolff-Boenisch, D., Gíslason, S.R., Oelkers, E.H., Putnis, C.V., 2004b. The dissolution of natural glasses as a function of their composition at pH 4 and 10.6, and temperatures from 25 to 74 °C. *Geochim. Cosmochim. Acta* 68, 4843–4858.
- Xu, T., Apps, J.A., Pruess, K., 2004. Numerical simulation to study mineral trapping for  $CO_2$  disposal in deep aquifers. *Appl. Geochem.* 19, 917–936.
- Xu, T., Apps, J.A., Pruess, K., 2005. Mineral sequestration of carbon dioxide in a sandstone shale system. *Chem. Geol.* 217, 295–318.
- Xu, T., Apps, J.A., Pruess, K., Yamamoto, H., 2007. Numerical modeling on injection and mineral trapping of  $CO_2$  with  $H_2S$  and  $SO_2$  in a sandstone formation. *Chem. Geol.* 242, 319–346.
- Xu, T., Sonnenthal, E.L., Spycer, N., Pruess, K., 2006. TOUGHREACT – a simulation program for non-isothermal reactive geochemical transport in variably saturated geological media. *Comp. Geosci.* 32, 145–165.
- Zerai, B., Saylor, B.Z., Matiso, G., 2006. Computer simulation of  $CO_2$  trapped through mineral precipitation in the Rose Run Sandstone. *Ohio. Appl. Geochem.* 21, 223–240.
- Ziemniak, S.E., Jones, M.E., Combs, K.E.S., 1993. Solubility behavior of titanium(IV) oxide in alkaline media at elevated temperatures. *J. Sol. Chem.* 22, 601–623.